LETTER

Anomalous metallic conductivity and short-range ferromagnetic correlation in high-pressure synthesized pyrochlore $Hg_2Ir_2O_7$

To cite this article: Jianfa Zhao *et al* 2024 *EPL* **145** 66001

A Letters Journal Exploring the Frontiers of Physics

March 2024

EPL, **145** (2024) 66001 www.epljournal.org
doi: 10.1209/0295-5075/ad2872

Anomalous metallic conductivity and short-range ferromagnetic correlation in high-pressure synthesized pyrochlore $Hg_2Ir_2O_7$

Jianfa Zhao[1], Zheng Deng[1(a)], Jun Zhang[1], Yi Peng[1], Luchuan Shi[1], Baosen Min[1], Lei Duan[1], Wenmin Li[1], Lipeng Cao[1], Jeng-Lung Chen[2], Zhiwei Hu[3], Runze Yu[4] and Changqing Jin[1(b)]

[1] *Beijing National Laboratory for Condensed Matter Physics, Institute of Physics, Chinese Academy of Sciences Beijing 100190, China*
[2] *National Synchrotron Radiation Research Center (NSRRC) - 101 Hsin-Ann Road, Hsinchu 30076, Taiwan*
[3] *Max-Planck Institute for Chemical Physics of Solids - Nothnitzer Straße 40, Dresden 01187, Germany*
[4] *Center for High Pressure Science & Technology Advanced Research - Beijing 100094, China*

received 21 November 2023; accepted in final form 12 February 2024
published online 20 March 2024

Abstract – Iridates show fascinating properties due to the unpredictable ground states of their Ir cations. Generally, $Ir^{5+}(5d^4)$ systems exhibit insulating nonmagnetic states owing to the strong spin-orbit coupling (SOC). Herein a new pyrochlore iridate $Hg_2Ir_2O_7$ with an Ir^{5+} charge state synthesized by high-pressure technique is reported. $Hg_2Ir_2O_7$ crystallizes in the typical cubic pyrochlore crystal structure. The Ir^{5+} valence state is evidenced by the XAS spectrum. Surprisingly, $Hg_2Ir_2O_7$ displays short-range ferromagnetic correlations at low temperatures as evidenced by *S*-shape field-dependent magnetization curves, positive magnetoresistance, and magnetic excitations in specific heat. Furthermore, it also shows metallic conduction and large electron component of specific heat. These results all indicate that Ir^{5+} in $Hg_2Ir_2O_7$ deviates from SOC-dominated insulating nonmagnetic states.

Introduction. – Iridates have been attracting substantial attention due to the fascinating properties of 5*d* electrons that are emergent from competition between Coulomb repulsion energy, spin-orbit coupling (SOC), and crystalline electric field (CEF) energy [1–4]. Antiferromagnetic insulator Sr_2IrO_4 with $Ir^{4+}(5d^5)$ shows SOC-dominated $j_{eff} = 1/2$ Mott state [5]. The family of rare-earth $RE_2Ir_2O_7$ (RE = from Nd to Lu) with $Ir^{5+}(5d^4)$ exhibits metal/semiconductor-to-insulator transitions (MIT) with decreasing temperature [6–8]. The insulating state seems to be induced by the magnetic ordering of the Ir sublattice, and the transition temperatures moving to higher values were observed from A = Nd to Lu [8–11]. The reason is that magnetic ordering is influenced by interatomic distances and the change in the Ir-O-Ir angle, which are in turn connected to the size of rare-earth cations [6,7]. Additionally, the strong spin-orbit coupling of 5*d*-electron and weak electron correlations between extended 5*d*-orbitals in these $RE_2Ir_2O_7$ could generate various complex states, *e.g.*, topological phases, Weyl semi-metal or topological Mott insulator [7,12–16].

On the other hand, $Ir^{5+}(5d^4)$ systems display unique features. For iridates, the strong SOC splits t_{2g} orbitals into a twofold $j_{\rm eff} = 3/2$ band with lower energy and a single $j_{\rm eff} = 1/2$ band with higher energy [17]. In such a scenario the Ir^{5+} iridate has a fully occupied $j_{\rm eff} = 3/2$ band and an empty $j_{\rm eff} = 1/2$ band, resulting in a well-defined nonmagnetic insulating state. $NaIrO_3$, Sr_2YIrO_6 follow the above mechanism [18,19], while recently found pyrochlore $Cd_2Ir_2O_7$ showed opposite behavior [20]. The latter shows metallic conduction with short-range ferromagnetic correlations rather than the nonmagnetic insulating behavior. This anomaly is attributed to the competition between SOC and non-negligible CEF energy. The latter is produced by significant structural distortions of IrO_6 octahedra.

The relatively smaller size of the Cd^{2+} ion (0.95 Å) resulted in significant structural distortions in $Cd_2Ir_2O_7$, it would be interesting to have a larger divalent cation to replace Cd to generate no or moderate structural distortions in a new pyrochlore analog. With proper comparison, one could have a deeper insight into the metallic state of Ir^{5+} in pyrochlore iridates. In this work, a new pyrochlore iridate $Hg_2Ir_2O_7$ was synthesized with high-temperature and high-pressure techniques. The Hg ion with a single valence

(a) E-mail: dengzheng@iphy.ac.cn (corresponding author)
(b) E-mail: jin@iphy.ac.cn (corresponding author)

state of +2 and a larger size of 1.02 Å was selected as A site cation to ensure the Ir^{5+} configuration. The new material also shows short-range ferromagnetic correlations at low temperatures. It presents more metallic conducting properties but moderate structural distortions of IrO_6 octahedra, compared to analog $Cd_2Ir_2O_7$. Our work implies that in addition to the structural distortions of IrO_6 octahedra, there must be other potential factors to tune Ir^{5+} band structure.

Experiment. – The polycrystalline sample $Hg_2Ir_2O_7$ was synthesized with the high-pressure and high-temperature technique as described in detail elsewhere [21–25]. Standard reagents, HgO (99.9%), IrO_2 (99.9%), and $KClO_4$ (99.9%, as an oxidizing agent) powders, with molar ratio of $HgO:IrO_2:KClO_4 = 2:2:1$ were mixed and synthesized under 5 GPa and 1373 K for 30 min. Extra $KClO_4$ was used to ensure the complete oxidization of Ir^{5+} in the title compound. The oxidizing agent $KClO_4$ plays an important role in the high-pressure synthesis [26]. It is worth noting that if $KClO_4$ (or other oxidizing agent) were not added to the starting materials before synthesis, HgO and IrO_2 would be recovered without any reaction. The recovered product was washed out by de-ionized water to exclude residual KCl. Phase purity and crystal structure were determined with laboratory powder X-ray diffraction (XRD) at room temperature. We performed continuous scanning using Cu-$K_{\alpha 1}$ radiation over a range between 10° and 100° with steps of 0.005°. The Rietveld refinement of XRD data was conducted with the GSAS program [27]. The hard X-ray absorption spectroscopy (XAS) of the Ir-L_3 edge was measured in the transmission geometry at the beamline of BL17C at the National Synchrotron Radiation Research Center (NSRRC) in Taiwan. Resistivity (ρ) and specific heat (C_p) measurements were performed with a physical property measurement system. The magnetization measurements were performed with a superconducting quantum interference device magnetometer (Quantum Design).

Results. – Figure 1(a) shows the XRD pattern and the corresponding refinement of $Hg_2Ir_2O_7$. A small amount of IrO_2 (<1% in weight) can be found at 28°, 40°, 54°, etc., as shown by green bars in fig. 1(a). The sample crystallizes into a typical cubic pyrochlore structure with the space group of Fd-$3m$ (No. 227) as shown in fig. 1(b). We obtained structural parameters using the Rietveld refinement. The obtained parameters are listed in table 1. Since the conducting behavior and magnetic properties are mainly influenced by IrO_6 octahedra, the configuration of IrO_6 octahedra is analyzed. It is worth noting that the only ligand oxygen of Ir is O_1, which is also the only variable atom in the lattice. The O-Ir-O bond angles are 89.80(3)° and 90.20(5)°, and the O-Ir bond length is 1.916(4) Å. The O-Ir-O bond angles slightly deviate from 90° of an ideal octahedron. However, the Ir-O-Ir bond angle which indicates the tilting between corner-sharing IrO_6 octahedra is only 140.77(1)°. A similar octahedral distortion was also found in the $Cd_2Ir_2O_7$ compound [20].

It is well known that the energy position of X-ray absorption near edge structure (XANES) at the 5d transition-metal $L_{2,3}$ edges is very sensitive to the valence state. The energy difference between two different valence states $5d^n$ ($n = 5$ for Ir^{4+}) and $5d^{n-1}$ (for Ir^{5+}) is $\Delta E = E(2p^6d^{n-1} \rightarrow 2p^5 5d^n) - E(2p^6 5d^n \rightarrow 2p^5 5d^{n+1}) \approx U_{pd} - U_{dd} \approx 1\,\mathrm{eV}$, where U_{dd} is the Coulomb repulsion energy between two 5d electrons and U_{pd} is the one between a 5d electron and the 2p core hole. Therefore, it is generally used to determine the valence states of 5d transition-metal ion [20,28,29]. Figure 1(c), shows the Ir-L_3 XANES of $Hg_2Ir_2O_7$ together with an Ir^{5+} reference Sr_2CoIrO_6 and an Ir^{4+} reference La_2CoIrO_6 with a similar IrO_6 octahedral coordination for comparison [17,30]. The latter was measured simultaneously for energy calibration. The energy position of the white line at the Ir-L_3 peak of $Hg_2Ir_2O_7$ shifts by 1.2 eV to higher energy relative to that of Ir^{4+} reference La_2CoIrO_6, but located at the same energies as that of Sr_2CoIrO_6, confirming Ir^{5+} valence state in $Hg_2Ir_2O_7$. We cannot completely rule out the possibility of a small part of Ir^{4+} impurity in the sample due to the low resolution of XANES for 5d elements. Nevertheless, we still argue that the anomalous behaviors of $Hg_2Ir_2O_7$ is from the majority Ir^{5+}, as discussed in the section of specific heat. It is noteworthy that Ir-L_3 peaks of $Hg_2Ir_2O_7$ and Sr_2CoIrO_6 show an asymmetric feature. The details of such spectral feature are more clearly to be seen in the second derivative of the $Hg_2Ir_2O_7$ spectrum as shown in fig. 1(c). The splitting in the second derivative can be assigned to crystal field splitting for t_{2g} and e_g orbitals which is usually 2.5–3 eV for 5d elements. Here, the second derivative of Ir ion in $Hg_2Ir_2O_7$ splits into two peaks with energy difference of about 2.5 eV. A similar phenomenon was reported in Sr_2MIrO_6 (M = Sc, Fe, In) with Ir^{5+} ions [31].

Figure 2(a) shows the temperature dependence of susceptibility (χ) for $Hg_2Ir_2O_7$ after zero-field-cooling (ZFC) and field-cooling (FC) processes under an external field of 0.1, 1, and 7 T. It is worth noting that the differences between ZFC and FC of 1 and 7 T are negligible as shown in fig. 2(a). No visible magnetic phase transition can be observed down to 2 K. Between 100 and 300 K, the susceptibility is nearly temperature-independent [32,33]. On the other hand, we found that the paramagnetic susceptibility in the temperature range of 300–400 K can be well fitted with the Curie-Weiss law as shown in fig. 2(b). A modified Curie-Weiss fitting ($\chi - \chi_0 = C/T - \theta$) was used for fitting, where χ_0 is from Pauli paramagnetic contribution. A similar method was used for Sr_2IrO_4 and $Cd_2Ir_2O_7$ [20]. The linear fitting yielded the temperature-independent susceptibility $\chi_0 = 3.9 \times 10^{-4}$ emu/mol/Oe, the Curie constant $C = 0.0228$ emu K/mol/Oe, and a large negative Weiss temperature of $\theta = -65$ K. χ_0 of the title material is comparable with that of Sr_2IrO_4 (8.8×10^{-4} emu/mol/Oe) [34] and $Sm_2Ir_2O_7$ ($\sim 1 \times 10^{-3}$ emu/mol/Oe) [7]. We can also

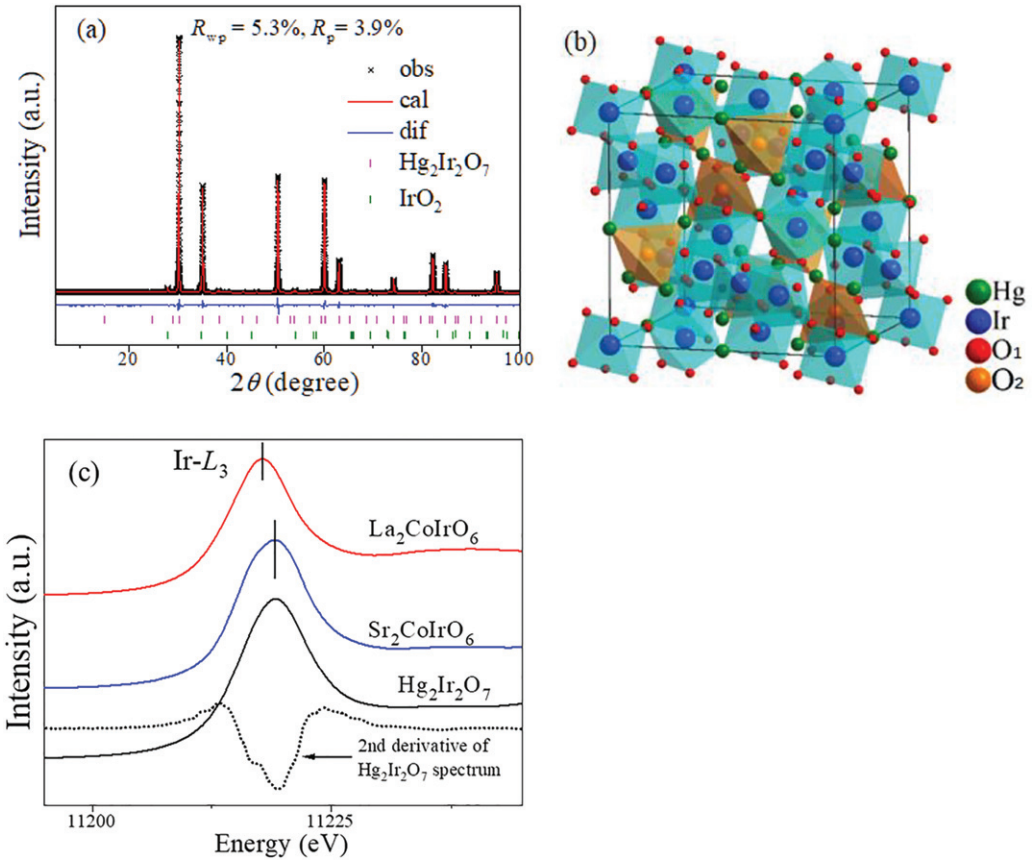

Fig. 1: (a) XRD spectrum and Rietveld refined profiles. (b) Crystal structure of $Hg_2Ir_2O_7$. (c) Ir-L_3 XANES spectra of $Hg_2Ir_2O_7$, $Sr_2CoIr^{5+}O_6$ and $La_2CoIr^{4+}O_6$ for comparison. The dotted line is the second derivative of the $Hg_2Ir_2O_7$ spectrum.

Table 1: Structural parameters as determined by Rietveld refinements.

Parameters	Value
T (K)	300
space group	Fd-3m
a (Å)	10.2101(1)
V (Å^3)	1064.374(3)
Hg	1/2, 1/2, 1/2
Ir	0, 0 ,0
O_1	0.3130(5), 1/8, 1/8
O_2	3/8, 3/8, 3/8
$l_{\text{Ir-O}}$ (Å)	1.916(4)
∠O-Ir-O (°)	87.80(3)/90.20(5)
∠Ir-O-Ir (°)	140.77(1)

obtain the effective moment $M_{\text{eff}} = 0.31\,\mu_B$/Ir. This value is smaller than that of magnetic Ir^{5+} compounds, *e.g.*, $0.91\,\mu_B$/Ir in antiferromagnet Sr_2YIrO_6 and $0.88\,\mu_B$/Ir for Ir^{4+} pyrochlore $Lu_2Ir_2O_7$ [35]. Yet another Ir^{4+} pyrochlore $Y_2Ir_2O_7$ [36] showed a more comparable M_{eff} of 0.54 μ_B/Ir. The remaining magnetic moment of Ir^{5+} in $Hg_2Ir_2O_7$ suggests that SOC is not strong enough but in some intermediate region. Thus, the electronic ground state of Ir^{5+} in the current $Hg_2Ir_2O_7$ apparently deviates from the SOC-dominated $J = 0$.

Correspondingly, one can find nonlinear field dependence of magnetization ($M(H)$) curves below 50 K in fig. 2(c). At higher temperatures, the $M(H)$ curves become linear as shown in fig. 2(d). The nonlinear behavior gradually increases and becomes unambiguous S-shape at 5 and 2 K, indicating the presence of the ferromagnetic component between Ir^{5+} cations [37]. The aforementioned strong SOC splits the Ir^{5+} orbital into a fully occupied $j_{\text{eff}} = 3/2$ band and an empty $j_{\text{eff}} = 1/2$ band, then the Ir^{5+} is supposed to have a nonmagnetic ground state. The presence of magnetic interaction at low temperatures distinguishes the electronic ground state of Ir^{5+} in $Hg_2Ir_2O_7$ from the SOC-dominated $J = 0$ state. Similar $M(H)$ curves were found in analog $Cd_2Ir_2O_7$ where the structural distortion of IrO_6 octahedra mixed $j_{\text{eff}} = 3/2$ and $j_{\text{eff}} = 1/2$ bands as demonstrated by density functional theory calculations [20]. As a similar structural distortion has been shown in fig. 1(b) and table 1, we can expect a comparable mixture of $j_{\text{eff}} = 3/2$ and $j_{\text{eff}} = 1/2$ bands. Thus, Ir^{5+} in $Hg_2Ir_2O_7$ is proposed to be a magnetic $J > 0$ state, due to competing SOC and CEF energy [20].

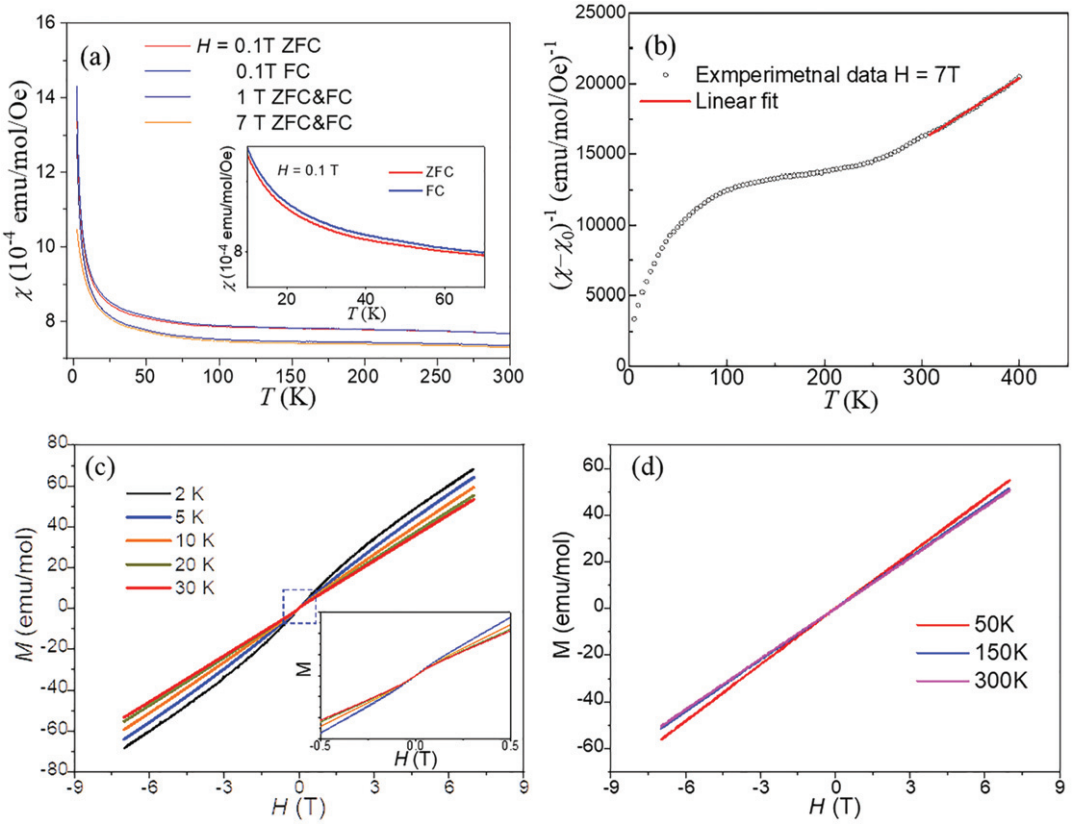

Fig. 2: (a) $\chi(T)$ curves of $Hg_2Ir_2O_7$ under measuring field of 0.1, 1, and 7 T after ZFC and FC. The inset is enlarged $\chi(T)$ of 0.1 T at low temperatures. (b) $1/\chi(T)$ curve and the corresponding Curie-Weiss fit of $Hg_2Ir_2O_7$ under measuring field of 7 T. $M(H)$ curves of $Hg_2Ir_2O_7$ at (c) $T = 2, 5, 10, 20$, and 30 K. The inset is the enlarged area of low fields. (d) $T = 50$, 150 and 300 K.

Figure 3(a) presents the resistivity (ρ) as a function of temperature. In the measuring temperature range, the change of resistivity is less than 10% compared to $\rho_{300\,\mathrm{K}}$. The resistivity shows a steady decrease with decreasing temperature from 300 to 100 K, where the magnetization is almost a constant coincidentally. With decreasing temperature, the resistivity gradually decrease above 100 K. Similar metallic conduction was found in $RE_2Ir_2O_7$, with well-defined Ir^{4+} [7,38,39]. Thus, the metallic conduction can also distinguish $Hg_2Ir_2O_7$ from the $J = 0$ state. Below 100 K, a gradual increase of resistivity with decreasing temperature suggests a possible metal-insulator transition (MIT). However, no corresponding change can be observed on $M(T)$ or temperature-dependent specific heat ($C_p(T)$ in fig. 3(c)). On the other hand, pronounced anomalies have been found in specific heat of $RE_2Ir_2O_7$. These anomalies are related rather to magnetic transitions, and the latter induce MIT in $RE_2Ir_2O_7$ [6,7]. Given the absence of visible magnetic transition, one could argue the nature of the possible MIT in $Hg_2Ir_2O_7$. It could be worth being investigated in the future. Magnetoresistance is usually related to magnetism in a metallic compound. We found clear positive magnetoresistance at low temperatures. As shown in fig. 3(b), $Hg_2Ir_2O_7$ has a magnetoresistance of about 0.5% below 10 K. The magnetoresistance gradually becomes smaller with increasing temperatures. Above 100 K, it becomes negligible. This unambiguous magnetoresistance at low temperatures supports the short-range FM correlation at low temperatures.

$C_p(T)$ also shows evidence of free carriers and magnetic interactions at low temperatures. It is worth noting that no visible anomaly can be found from 2 to 200 K as shown in fig. 3(c). Generally, two-components fitting is used to fit $C_p(T)$ data, which contains an electronic contribution and a lattice one. In this case, a linear behavior is expected for the curve of C_p/T *vs.* T^2 at low temperatures. However, $C_p/T(T^2)$ clearly deviates from a simple linear fitting as shown in fig. 3(d). Thus, a magnetic component is proposed to modify the fitting as $C_p = \gamma T + \beta T^3 + mT^{1.5}$, where γT is the free electronic contribution, βT^3 for the lattice, and $mT^{1.5}$ for some sort of short-range ferromagnetic excitations. The fitting yields $\gamma = 3.5\,\mathrm{mJ/mol/K^2}$, $\beta = 2.9\,\mathrm{mJ/mol/K^4}$ (*i.e.*, $\theta_\mathrm{D} = 194\,\mathrm{K}$) and $m = 3.2\,\mathrm{mJ/mol/K^{2.5}}$. Here γ is apparently larger than that of analog $Cd_2Ir_2O_7$ compound [20]. This large γ (free electronic contribution to specific heat) indicates a large number of free carriers near Fermi energy, which cannot only be attributed to minority

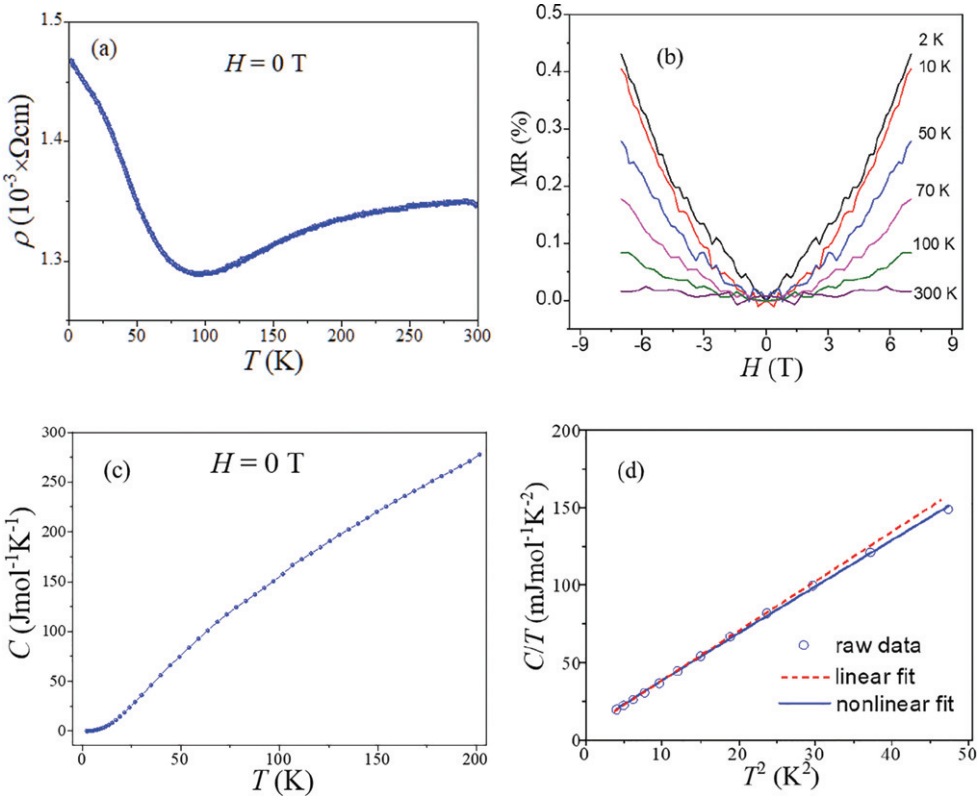

Fig. 3: (a) $\rho(T)$ curves of $Hg_2Ir_2O_7$ under measuring field of 0 T. (b) Positive magnetoresistance of $Hg_2Ir_2O_7$ at 2, 10, 50, 70, 100, and 300 K. (c) $C_p(T)$ curve of $Hg_2Ir_2O_7$ under measuring field of 0 T. (d) $C_p/T(T^2)$ and corresponding fitting curves of $Hg_2Ir_2O_7$ at low temperatures.

Ir^{4+} admixture. This large γ is consistent with the high conductivity, and again diverges Ir^{5+} in $Hg_2Ir_2O_7$ from the insulating $J = 0$ state.

Conclusions. – A new pyrochlore iridate $Hg_2Ir_2O_7$ was synthesized with high-pressure and high-temperature techniques. $Hg_2Ir_2O_7$ crystallizes in the typical cubic pyrochlore crystal structure. It contains weaker structural distortions of IrO_6 octahedra compared to analog $Cd_2Ir_2O_7$. The Ir^{5+} valence state is evidenced by the XAS spectrum, although we cannot compeletely rule out the possibility of a small amount of Ir^{4+} admixture in the sample. At low temperatures, the S-shape $M(H)$ curves, clear positive magnetoresistance, and the presence of magnetic excitations in specific heat results suggest the existence of magnetic interaction or short-range magnetic ordering. It is noteworthy that one could find the inconsistency between negative Weiss temperature and ferromagnetic-like S-like sharp of $M(H)$ curves. We believe that the net magnetic interaction between Ir cations is antiferromagnetic, but it still can tolerate some sort of ferromagnetic component. Resistivity and specific heat measurements indicate a metallic behavior of the Ir^{5+} state. We argue that despite of possible Ir^{4+} admixture, the metallic behavior of Ir^{5+} is still definite. The reason is that the large electron component of specific heat (3.5 mJ/mol/K^2) requires a large number of carriers which cannot only be attributed to minority Ir^{4+} admixture. Thus, the anomalous features of $Hg_2Ir_2O_7$ are mainly attributed to the Ir^{5+} ions. These results all indicate that Ir^{5+} in $Hg_2Ir_2O_7$ deviates from the nonmagnetic $J = 0$ state. Furthermore, $Hg_2Ir_2O_7$ has lower resistivity and larger electron component of heat capacity than the analog $Cd_2Ir_2O_7$, while the structural distortions in the latter is more significant. Thus, a new mechanism in addition to the structural distortions to influence Ir^{5+} electron configuration is expected based on our findings.

* * *

We acknowledge the support from the Max Planck-POSTECH-Hsinchu Center for Complex Phase Materials. The work was supported by Young Elite Scientists Sponsorship Program by CAST (Grant No. 2022QNRC001) and the National Natural Science Foundation of China (Grant Nos. 12204515, 12104488, 11974407). ZD acknowledges support of the Youth Innovation Promotion Association of CAS (No. 2020007) and CAS Project for Young Scientists in Basic Research (No. YSBR-030).

Data availability statement: All data that support the findings of this study are included within the article (and any supplementary files).

REFERENCES

[1] Kim B., Ohsumi H., Komesu T., Sakai S., Morita T., Takagi, H. and Arima T.-h., *Science*, **323** (2009) 1329.

[2] Jin H., Jeong H., Ozaki, T. and Yu J., *Phys. Rev. B*, **80** (2009) 075112.

[3] Jaubert L. D. and Holdsworth P. C., *Nat. Phys.*, **5** (2009) 258.

[4] Yu S., Peng Y., Zhao G., Zhao J., Wang X., Zhang J., Deng Z. and Jin C., *J. Semicond.*, **44** (2023) 032501.

[5] Kim B., Jin H., Moon S., Kim J.-Y., Park B.-G., Leem C., Yu J., Noh T., Kim C. and Oh S.-J., *Phys. Rev. Lett.*, **101** (2008) 076402.

[6] Stasko D., Vlaskova K., Proschek P. and Klicpera M., *J. Phys. Chem. Solids*, **176** (2023) 111268.

[7] Matsuhira K., Wakeshima M., Hinatsu Y. and Takagi S., *J. Phys. Soc. Jpn.*, **80** (2011) 094701.

[8] Klicpera M., Vlaskova K. and Divis M., *J. Phys. Chem. C*, **124** (2020) 20367.

[9] Vlášková, K., Colman R. and Klicpera M., *Mater. Chem. Phys.*, **258** (2021) 123868.

[10] Vlášková K., Diviš M. and Klicpera M., *J. Magn. & Magn. Mater.*, **538** (2021) 168220.

[11] Vlášková K., Proschek P., Diviš M., Le D., Colman R. H. and Klicpera M., *Phys. Rev. B*, **102** (2020) 054428.

[12] Taira N., Wakeshima M. and Hinatsu Y., *J. Phys.: Condens. Matter*, **13** (2001) 5527.

[13] Nakatsuji S., Machida Y., Maeno Y., Tayama T., Sakakibara T., Van Duijn J., Balicas L., Millican J., Macaluso R. and Chan J. Y., *Phys. Rev. Lett.*, **96** (2006) 087204.

[14] Machida Y., Nakatsuji S., Onoda S., Tayama T. and Sakakibara T., *Nature*, **463** (2010) 210.

[15] Das M., Bhowal S., Sannigrahi J., Bandyopadhyay A., Banerjee A., Cibin G., Khalyavin D., Banerjee N., Adroja D. and Dasgupta I., *Phys. Rev. B*, **105** (2022) 134421.

[16] Wan X. G., Turner A. M., Vishwanath A. and Savrasov S. Y., *Phys. Rev. B*, **83** (2011) 205101.

[17] Kolchinskaya A., Komissinskiy P., Yazdi M. B., Vafaee M., Mikhailova D., Narayanan N., Ehrenberg H., Wilhelm F., Rogalev A. and Alff L., *Phys. Rev. B*, **85** (2012) 224422.

[18] Du L., Sheng X., Weng H. and Dai X., *EPL*, **101** (2013) 27003.

[19] Cao G., Qi T., Li L., Terzic J., Yuan S., DeLong L. E., Murthy G. and Kaul R. K., *Phys. Rev. Lett.*, **112** (2014) 056402.

[20] Dai J. H., Yin Y. Y., Wang X., Shen X. D., Liu Z. H., Ye X. B., Cheng J. G., Jin C. Q., Zhou G. H., Hu Z. W., Weng S. C., Wan X. G. and Long Y. W., *Phys. Rev. B*, **97** (2018) 085103.

[21] Zhao J. F., Gao J. C., Li W. M., Qian Y. T., Shen X. D., Wang X., Shen X., Hu Z. W., Dong C., Huang Q. Z., Cao L. P., Li Z., Zhang J., Ren C. W., Duan L., Liu Q. Q., Yu R. C., Ren Y., Weng S.-C., Lin H.-J., Chen C.-T., Tjeng L.-H., Long Y. W., Deng Z., Zhu J. L., Wang X. C., Weng H. M., Yu R. Z., Greenblatt M. and Jin C. Q., *Nat. Commun.*, **12** (2021) 747.

[22] Deng Z., Kang C. J., Croft M., Li W. M., Shen X., Zhao J. F., Yu R. C., Jin C. Q., Kotliar G., Liu S. Z., Tyson T. A., Tappero R. and Greenblatt M., *Angew. Chem., Int. Ed.*, **59** (2020) 8240.

[23] Zhang J., Wang X., Zhou L., Liu G., Adroja D. T., da Silva I., Demmel F., Khalyavin D., Sannigrahi J. and Nair H. S., *Adv. Mater.*, **34** (2022) 2106728.

[24] Zhao J. F., Wang X., Shen X., Sahle C. J., Dong C., Hojo H., Sakai Y., Zhang J., Li W. M., Duan L., Chan T. S., Chen C. T., Falke J., Liu C. E., Kuo C. Y., Deng Z., Wang X. C., Yu R. C., Yu R. Z., Hu Z. W., Greenblatt M. and Jin C. Q., *Chem. Mater.*, **34** (2021) 97.

[25] Deng Z., Wang X., Wang M., Shen F., Zhang J., Chen Y., Feng H. L., Xu J., Peng Y. and Li W., *Adv. Mater.*, **35** (2023) 2209759.

[26] Zhao J. F., Haw, S.-C., Wang X., Hu Z. W., Kuo, C.-Y., Chen, S.-A., Ishii H., Hiraoka N., Lin, H.-J., Chen, C.-T., Li Z., Tanaka A., Liu C. E., Yu R. Z., Chen J. M. and Jin C. Q., *Phys. Status Solidi B*, **258** (2021) 2100117.

[27] Toby B. H., *J. Appl. Crystallogr.*, **34** (2001) 210.

[28] Baroudi K., Yim C., Wu H., Huang Q., Roudebush J. H., Vavilova E., Grafe, H.-J., Kataev V., Buechner B. and Ji H., *J. Solid State Chem.*, **210** (2014) 195.

[29] Feng H. L., Calder S., Ghimire M. P., Yuan, Y.-H., Shirako Y., Tsujimoto Y., Matsushita Y., Hu Z., Kuo, C.-Y. and Tjeng L. H., *Phys. Rev. B*, **94** (2016) 235158.

[30] Agrestini S., Chen K., Kuo C.-Y., Zhao L., Lin H.-J., Chen C.-T., Rogalev A., Ohresser P., Chan, T.-S. and Weng S.-C., *Phys. Rev. B*, **100** (2019) 014443.

[31] Laguna-Marco M. A., Kayser P., Alonso J. A., Martínez-Lope M. J., van Veenendaal M., Choi Y., Haskel D., *Phys. Rev. B*, **91** (2015) 214433.

[32] Liu X., Riney L., Guerra J., Powers W., Wang J., Furdyna J. K. and Assaf B. A., *J. Semicond.*, **43** (2022) 112502.

[33] Wei Q., Wang H., Zhao X. and Zhao J., *J. Semicond.*, **43** (2022) 072101.

[34] Cao G., Bolivar J., McCall S. and Crow J. E., *Phys. Rev. B*, **57** (1998) R11039.

[35] Klicpera M., Vlášková, K. and Diviš, M., *J. Magn. & Magn. Mater.*, **506** (2020) 166793.

[36] Liu H., Liang D., Chen S., Bian J., Feng Y. and Fang B., *Wuhan University Journal of Natural Sciences*, **22** (2017) 215.

[37] Zhao X., Dong J., Fu L., Gu Y., Zhang R., Yang Q., Xie L., Tang Y. and Ning F., *J. Semicond.*, **43** (2022) 112501.

[38] Feng H. L., Kang, C.-J., Deng Z., Croft M., Liu S., Tyson T. A., Lapidus S. H., Frank C. E., Shi Y. and Jin C., *Inorg. Chem.*, **60** (2021) 4424.

[39] Matsuhira K., Wakeshima M., Nakanishi R., Yamada T., Nakamura A., Kawano W., Takagi S. and Hinatsu Y., *J. Phys. Soc. Jpn.*, **76** (2007) 043706.